ACS OMEGA

http://pubs.acs.org/journal/acsodf

Article

# Synthesis and Characterization of $Ag/Al_2O_3$ Catalysts for the Hydrogenation of 1-Octyne and the Preferential Hydrogenation of 1-Octyne vs 1-Octene

Revana Chanerika, Mzamo L. Shozi, and Holger B. Friedrich*

Cite This: *ACS Omega* 2022, 7, 4026−4040

Read Online

ACCESS | Metrics & More | Article Recommendations | Supporting Information

**ABSTRACT:** Catalysts featuring 2, 5, and 10 wt % silver supported on alumina were prepared by the deposition precipitation method and activated under hydrogen. All catalysts were characterized by Brunauer−Emmett−Teller (BET) measurements, inductively coupled plasma-optical emission spectrometry (ICP-OES), backscattered electron scanning electron microscopy (BSE-SEM), high-resolution transmission electron microscopy (HR-TEM), hydrogen-temperature-programmed reduction ($H_2$-TPR), $H_2$-chemisorption, thermogravimetric analysis (TGA), infrared (IR) spectroscopy, X-ray diffraction (XRD), Raman spectroscopy, and isopropylamine (IPA) TPD and evaluated in a continuous plug flow fixed-bed reactor. Metal nanoparticles with average sizes of 4.5, 11.5, and 21.1 nm were identified by HR-TEM for the 2, 5, and 10 wt % $Ag/Al_2O_3$ catalysts, respectively. A conversion of 99% was observed for 1-octyne over particles between 10 and 15 nm in size, with stable operation up to 24 h (decreasing thereafter) at a temperature of 140 °C and a pressure of 30 bar in the competitive hydrogenation reaction. No conversion of 1-octene was noted in competitive reactions (mixed 1-octyne and 1-octene feed) but rather a gain of 1-octene throughout the 72 h time-on-stream. The performance of all catalysts was influenced by both the metal and support, where the latter impacted the overall acidity of the catalysts, thus affecting their long-term stability.

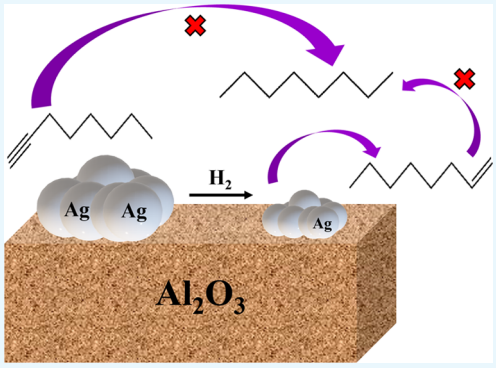


## 1. INTRODUCTION

Alkenes are an important class of raw materials used in various fields of industrial organic synthesis. For example, ethylene is used in producing polyethylene, poly(vinyl chloride), ethanol, ethylene oxide, acetaldehyde, vinyl acetate, and polymers thereof.[1] In industries, the selective hydrogenation process is mainly utilized to produce value-added compounds or intermediates and to remove acetylenic compounds, which are problematic impurities in, e.g., polymer processes, where operational problems such as deactivation by plugging result.[2] For this reason, it is important that alkyne impurities be reduced to a minimum admissible value between 1, 2, 5, and even 10 ppm depending on the final processing product.[3−5]

Unsaturated hydrocarbons are commonly produced through thermal, steam, or catalytic cracking of petroleum alkanes.[1,6] High temperatures are ideal for heavy hydrocarbon cracking, and this can usually occur without the participation of a catalyst. Light alkenes, like ethylene and propylene, are typical products of this process, which inevitably include alkynes and dienes.

Fractional distillation is typically utilized to remove such impurities. However, the process itself requires high energy and capital expenditures. Therefore, the selective hydrogenation of alkynes and dienes is, so far, the most promising method of purification of alkenes in the presence of these impurities.[3−5] To improve the efficiency and selectivity of the hydrogenation reaction, task-specific approaches should be considered to satisfy the following criteria:[7]

i. High catalytic activity targeting almost 100% conversion of the impurity.
ii. High alkene selectivity (between 95 and 99% and not below 80%).
iii. Long-term catalyst stability throughout the reaction.
iv. Insensitivity of the catalyst to poisoning.
v. Ease of preparation and regeneration of the catalyst.

Over the last few decades, research has shown that the hydrogenation of highly unsaturated hydrocarbons can be successfully implemented over supported metal catalysts in which d-block metals serve as the active components. Metals such as palladium,[3,8−14] nickel,[15] platinum,[16] copper,[17] silver,[18] gold,[19,20] rhodium,[21] and cobalt[17] have all been found to be active in the hydrogenation. Supported heterogeneous catalysts

Received: September 21, 2021
Accepted: November 19, 2021
Published: January 26, 2022

incorporating palladium have thus far shown to be most active and durable. As a result, the majority of publications, when discussing the mechanism of catalytic action in the hydrogenation of acetylenes, use Pd catalytic systems.

It has been found in many catalysis studies that the hydrogenation of the alkyne to the alkene is more favored than the overhydrogenation reaction to the alkane as a result of the higher adsorption coefficient of alkynes compared to alkenes.[22] Thus, hydrogenation of alkynes to alkenes dominates over the hydrogenation of alkenes to alkanes under conditions of sorption equilibria. In the case of the Lindlar catalyst, with a higher sorption affinity of the alkyne to Pd than that of alkene, a faster alkene desorption from the surface of Pd is expected at the instant of formation, thus preventing the overhydrogenation with this alkene.[23] Since the Lindlar catalyst contains lead, many replacements have been sought to eliminate catalyst deactivation caused by poisoning of palladium by lead during the hydrogenation process.

Research has shown that silver has a low affinity toward hydrogen due to its filled d-band compared to metals like nickel, palladium, and platinum. According to theoretical calculations, hydrogen interacts weakly with extended metal surfaces such as single crystals and polycrystalline surfaces and no dissociative chemisorption occurs at low reaction temperatures as a result of the filled d-band of silver. Silver can thus be considered as one of the most powerful carbon−carbon $\pi$-triple bond activators due to its $d^{10}$ electron configuration.[24]

A catalyst for the selective hydrogenation of alkynes should possess chemical, sorption, and texture properties aimed at ensuring the highest rate possible for the hydrogenation of the alkyne to alkene (**1**), while minimizing the undesired pathways that include the sequential hydrogenation of the alkene to the alkane (**2**), direct hydrogenation of the alkyne to the alkane (**3**), and production of oligomeric materials from the alkyne **4** (Scheme 1).

**Scheme 1. Competitive Hydrogenation of Acetylene and Its Homologues**

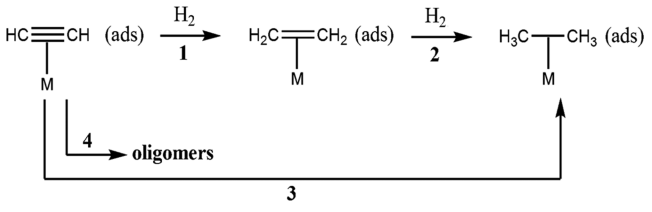


Recently, studies have focused on making catalysts with nanoparticles of the metals to enhance the catalytic activity. To be successful, the catalyst must allow the reaction to proceed at a suitable rate under economically desirable conditions, at as low temperatures and pressures as possible. It must also be long-lasting. Taking these factors into account, this study focuses on Ag catalysts that function under environmentally benign conditions, while limiting the amount of waste produced and energy consumed.

1-Octene provides special features such as elasticity, flexibility, impact resistance, and strength to plastic consumer products and is in high demand. Thus, the rationale of this study is to remove homogeneous catalyst poisons, such as alkynes from an octene stream (which would otherwise cause severe catalyst deactivation downstream), and to hydrogenate 1-octyne to the value-added 1-octene, in the presence of 1-octene using a continuous flow fixed-bed reactor (Figure S1).

It is hypothesized that the use of Ag supported on alumina (characterized by high surface area, porosity, and high thermal and mechanical stabilities) will give selective catalysts, which can function under mild reaction conditions which are industrially viable. No literature exists on the hydrogenation of 1-octyne over Ag catalysts.

## 2. RESULTS AND DISCUSSION

**2.1. Characterization.** *2.1.1. Scanning Electron Microscopy-Energy Dispersive X-ray (SEM-EDX).* Figure 1 shows the surface structure of the 2, 5, and 10 wt % $Ag/Al_2O_3$ catalysts using a scanning electron microscope with a backscattered electron (BSE) detector. From the maps combining silver and aluminum (map (d)), there are clear regions of silver enrichment in the $10Ag/Al_2O_3$ catalyst due to the higher content of silver loaded. There is also spatial coverage of the metal over the support (closer to the edges) and some silver agglomerates have formed, hence decreasing the metal dispersion over the carrier. With the $2Ag/Al_2O_3$ sample, the silver is more spatially distributed across the alumina, exposing more of the bare support as a result of the low metal loading (scattered distribution). The $5Ag/Al_2O_3$ catalyst appears to have well and evenly dispersed silver across the support with the least amount of regions of clustering compared to the $10Ag/Al_2O_3$ sample and also has the least amount of exposed support in comparison to the 2 and 10 wt % $Ag/Al_2O_3$ samples.

*2.1.2. Scanning Transmission Electron Microscopy (STEM)-EDX.* STEM/EDX imaging was used to determine the particle size and distribution of silver particles supported over alumina. Figure 2a−c shows BSE micrographs of the 2, 5, and 10 wt % $Ag/Al_2O_3$, respectively. Diameters of silver particles in nanometers were calculated assuming spherical particle shapes. The particles were found to distribute with relative uniformity across the surface of the alumina and agree with the SEM results previously discussed. A wide Ag particle size distribution with non-uniform shapes was observed especially in the $5Ag/Al_2O_3$ and $10Ag/Al_2O_3$ samples, where there are regions that contain slight (Figure 2b) and intense (Figure 2c) clustering of silver, as expected. In Figure 2c, some small Ag particles aggregated into larger ones. Using histograms of 100 particles each, the average silver particle sizes of $5Ag/Al_2O_3$ and $10Ag/Al_2O_3$ were calculated to be 11.5 and 21.1 nm, respectively (Figure 2e,f).

The average particle size of $2Ag/Al_2O_3$ is seen to be much smaller at 4.5 nm (Figure 2d) than those of the $5Ag/Al_2O_3$ and $10Ag/Al_2O_3$ samples, presenting a narrower distribution of the silver particle size with more uniform shapes (spherical) compared to the $5Ag/Al_2O_3$ and $10Ag/Al_2O_3$ catalysts. Also, there is a large fraction of Ag in a highly dispersed state (isolated ions). If it is assumed that the ratio between step and terrace silver atoms is dependent on particle size,[25] then it can be concluded that the 2 wt % sample contains a considerably higher fraction of low-coordinated silver atoms compared to the 5 and 10 wt % samples.

The particle size measurements from chemisorption and HR-TEM are very similar (Table S1). The HR-TEM and X-ray diffraction (XRD) data (Figure S2) strongly suggest that the Ag species are well dispersed on the 2 and 5 wt % $Ag/Al_2O_3$ samples but not on the 10 wt % $Ag/Al_2O_3$ catalyst.



https://doi.org/10.1021/acsomega.1c05231
ACS Omega 2022, 7, 4026−4040

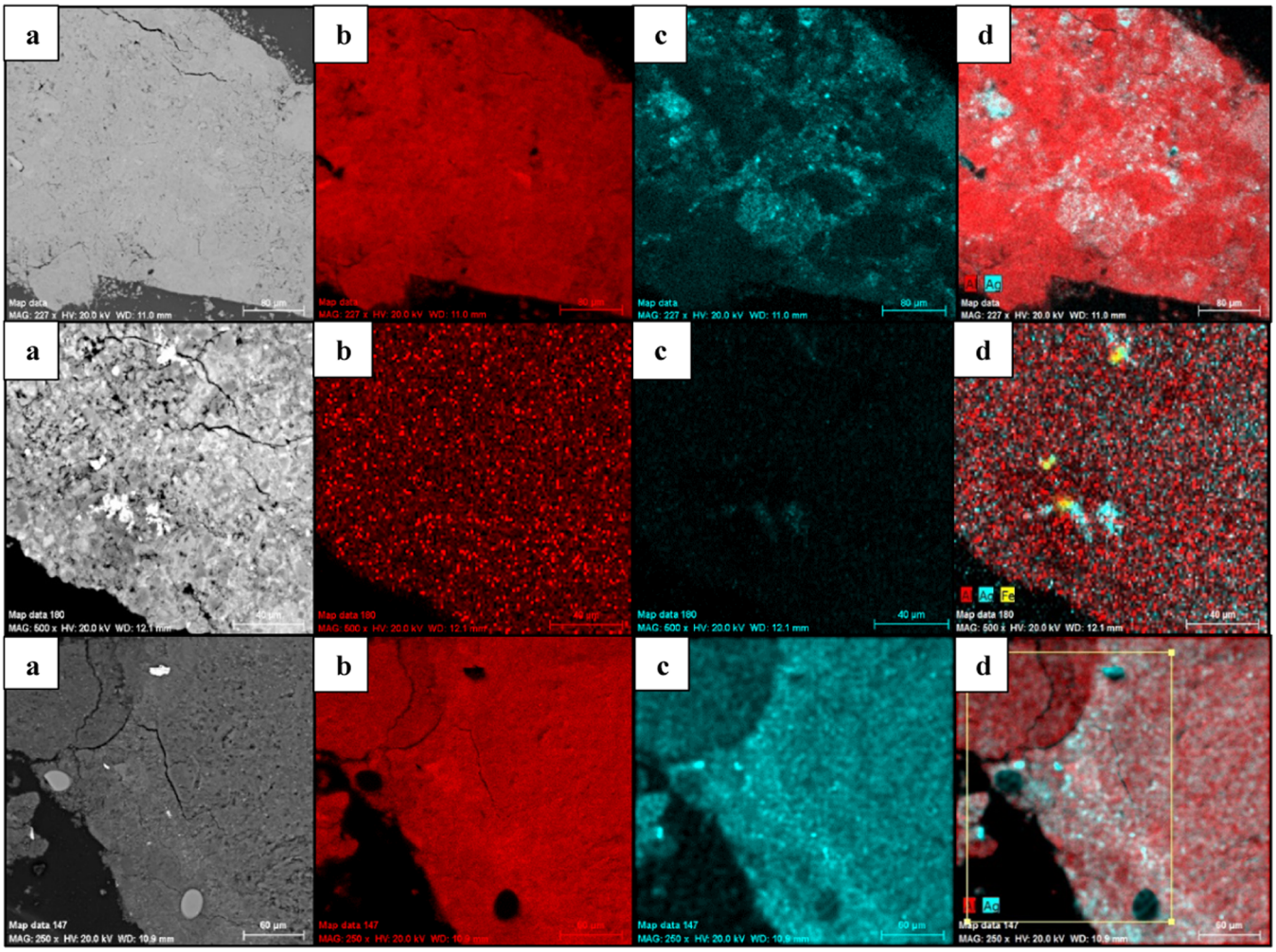


**Figure 1.** SEM-EDX images for 2 wt % (top), 5 wt % (middle), and 10 wt % (bottom) $Ag/Al_2O_3$ catalysts showing (a) dark-field image, (b) aluminum map, (c) silver map, and (d) silver and aluminum map.

*2.1.3. Hydrogen-Temperature Programmed Reduction ($H_2$-TPR).* $H_2$-TPR experiments were conducted to investigate the reducibility of the $Ag/Al_2O_3$ catalysts, and the results are shown in Figure 3 and Table 1. The cumulative $H_2$ reduction peaks were deconvoluted by searching for the optimal combination of Gaussian bands with correlation coefficients ($R^2$ values) above 0.99. Since large metal oxide clusters are easier to reduce than small metal oxide clusters or ions, and as bulk $Ag_2O$ is known to readily reduce,[26] the low-temperature peaks in the $H_2$-TPR profiles (Figure 3) of the 2, 5, and 10 wt % $Ag/Al_2O_3$ catalysts were assigned to the reduction of large AgO and $Ag_2O$ clusters, while the higher-temperature reduction peaks were assigned to well-dispersed silver oxide clusters or ions.[27]

At temperatures of 133, 120, and 200 °C for $2Ag/Al_2O_3$, $5Ag/Al_2O_3$ and $10Ag/Al_2O_3$, respectively, the reduction of surface oxygen on Ag is dominant (peak 1).[28] Peak 2 is assigned to the reduction of large AgO clusters, while peak 3 is due to the reduction of small and well-dispersed $Ag_2O$ particles. At high reduction temperatures, around 417−646 °C, in all three catalysts (peak 4), isolated AgO clusters reduce, while peak 5 (approximately 460−680 °C) was assigned to stable and well-dispersed $Ag^+$ ($Ag_2O$) ions.

Also, it is evident that Ag oxide species were present on all catalysts from the degree of reduction values calculated, which are in the range of 81−88% (Table 1). With increasing $Ag_2O$ species (with an increase in Ag content), the hydrogen consumption was seen to increase relative to the amount of silver loaded (Table 1). With weak metal−support interactions, large metal oxide (AgO) clusters are expected to be present. This was observed in the 10 wt % $Ag/Al_2O_3$ catalyst indicating the formation of large particles due to the content of silver loaded. In the same instance, the reduction of a large quantity of $Ag_2O$ species, shown by the highest peak area and intensity in the series of catalysts, to the metallic state is easier over the $2Ag/Al_2O_3$ due to the low Ag content.[27]

The XRD profiles in Figure S2 show the absence of AgO and $Ag_2O$ species confirming that the reduction conditions used to avoid sintering of silver (160 °C) were suitable for reducing the oxidized silver species to metallic silver, which is the active phase for the alkyne hydrogenation reactions.

**2.2. Noncompetitive Hydrogenation of Octyne.** The hydrogenation of octyne alone, in a noncompetitive process, was carried out to ascertain optimum parameters for testing in the competitive hydrogenation of octyne in the presence of octene. From the characterization techniques employed, the $5Ag/Al_2O_3$ catalyst seemed most promising (in terms of particle size, dispersion, and distribution) and was investigated in both noncompetitive and competitive hydrogenation


https://doi.org/10.1021/acsomega.1c05231
ACS Omega 2022, 7, 4026−4040

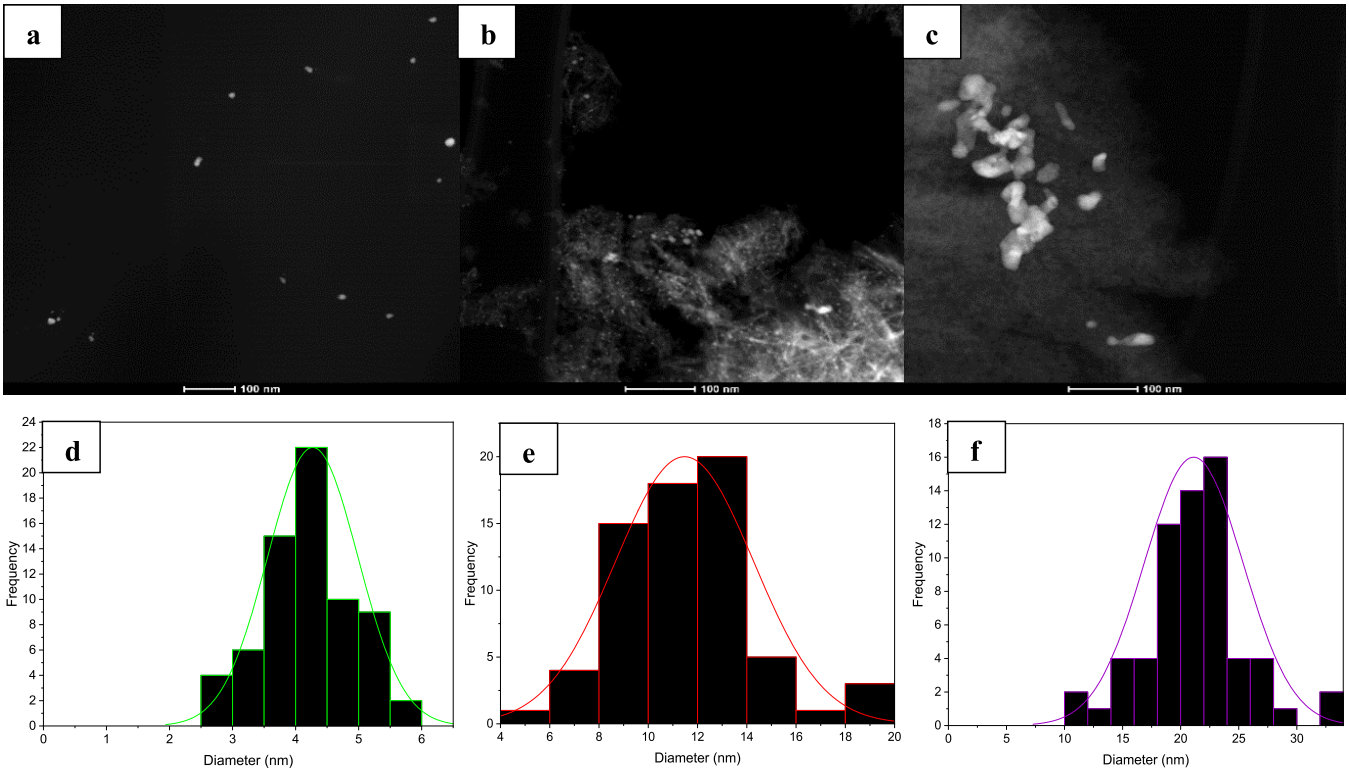


**Figure 2.** STEM-EDX images of (a) $2Ag/Al_2O_3$, (b) $5Ag/Al_2O_3$, and (c) $10Ag/Al_2O_3$ catalysts and (d–f) their respective particle size distribution graphs.

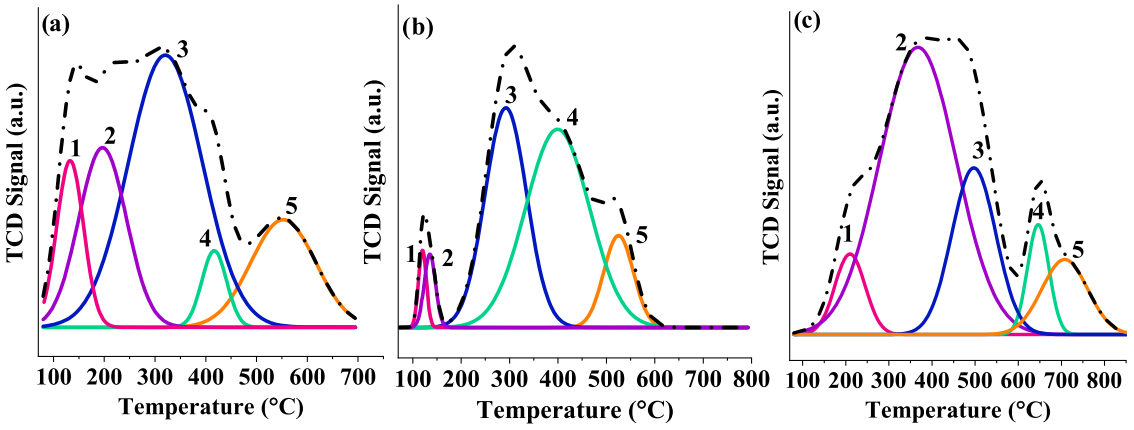


**Figure 3.** $H_2$-TPR profiles of (a) $2Ag/Al_2O_3$, (b) $5Ag/Al_2O_3$, and (c) $10Ag/Al_2O_3$ catalysts.

**Table 1. $H_2$-TPR Data of the $Ag/Al_2O_3$ Catalysts**

| | reduction temperature (°C) | | | | | | | |
|---|---|---|---|---|---|---|---|---|
| catalyst | peak 1 (°C) | peak 2 (°C) | peak 3 (°C) | peak 4 (°C) | peak 5 (°C) | peaks 2–5 $H_2$ consumption ($\mu$mol/g) | total $H_2$ consumption ($\mu$mol/g) | % $DR_T$[a] |
| $2Ag/Al_2O_3$ | 133 | 197 | 320 | 417 | 553 | 132.0 | 158.0 | 84 |
| $5Ag/Al_2O_3$ | 120 | 135 | 292 | 400 | 525 | 69.8 | 79.5 | 88 |
| $10Ag/Al_2O_3$ | 200 | 367 | 497 | 646 | 708 | 182.3 | 226.1 | 81 |

[a]$DR_T$ = ratio of hydrogen consumed for the reduction of silver oxides to the total hydrogen consumed from ambient temperature to 800 °C.

reactions and, hence, was chosen as the baseline catalyst for all optimization studies.

*2.2.1. Time-on-Stream Studies—Temperature Effects on Octyne Hydrogenation over $5Ag/Al_2O_3$.* Often in alkyne hydrogenation, the catalyst surface is covered almost immediately by carbonaceous deposits once exposed to hydrocarbons. The initial deposition is known to be temperature-dependent.[29] It is also common for heavy hydrocarbons to form and remain on the catalyst surface. To examine the effect of temperature, while minimizing the occurrence of side reactions by maintaining minimal contact time between the reactant feed and the catalyst bed, fixed conditions such as an



https://doi.org/10.1021/acsomega.1c05231
ACS Omega 2022, 7, 4026–4040

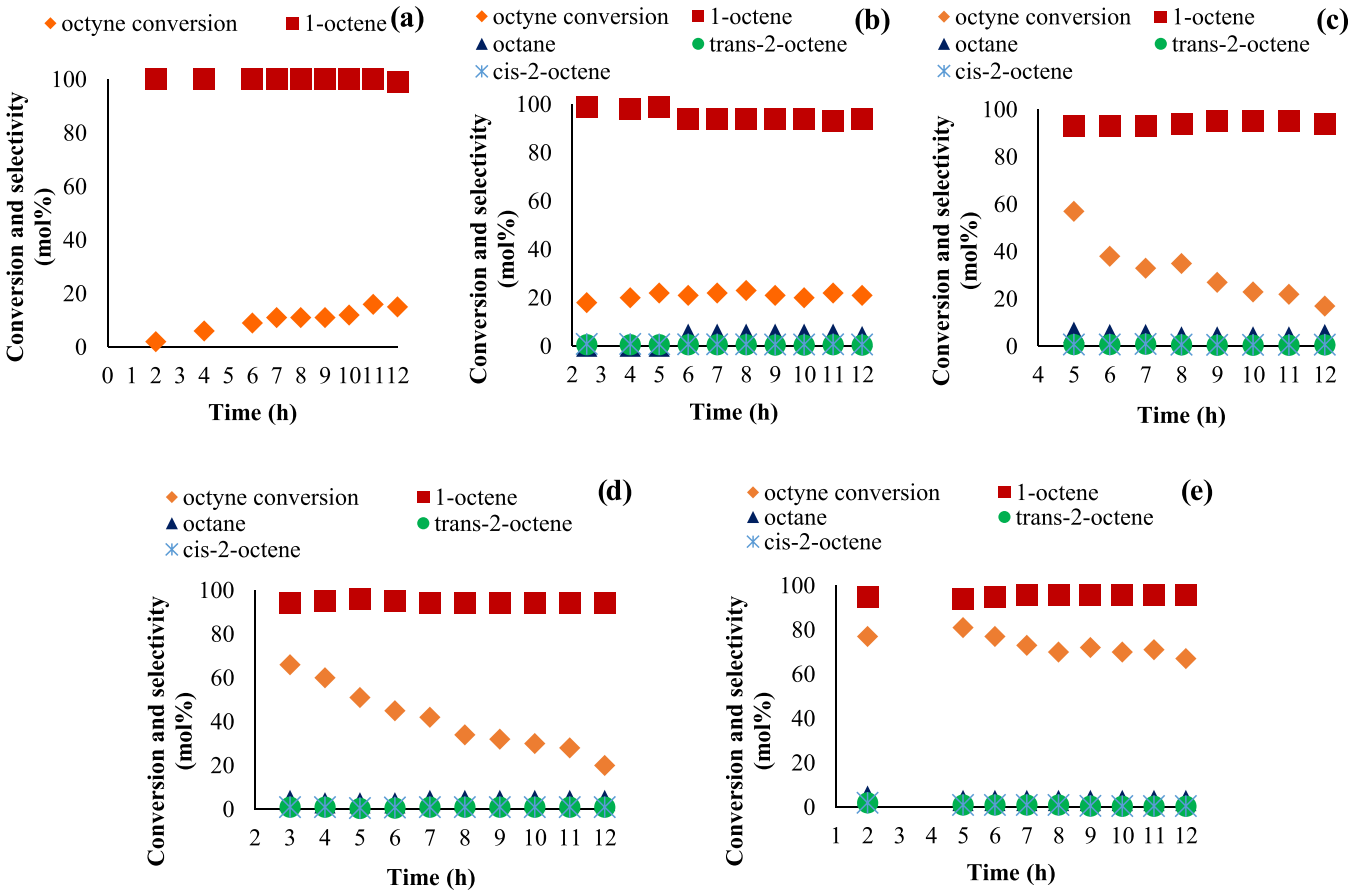


**Figure 4.** Conversion of octyne and selectivity to 1-octene, octane, *cis*-2-octene, and *trans*-2-octene at (a) 40 °C, (b) 80 °C, (c) 100 °C, (d) 120 °C, and (e) 140 °C over 5Ag/$Al_2O_3$. Reaction conditions: LHSV: 27 $h^{-1}$, pressure: 10 bar, octyne/$H_2$ ratio: 1:1.5, feed: 2 wt % octyne in hexane. The standard deviation for values at 12 h is ±1.5 mol %.

LHSV of 27 $h^{-1}$, 10 bar pressure, and an octyne/$H_2$ ratio of 1:1.5 were maintained. At low temperatures, 40 °C (Figure 4a), the retained carbon species (discussed in the next section of this report) decreased the hydrogenation rate of octyne. Therefore, low conversions were observed. Furthermore, the non-steady-state behavior has been well documented to be due to the growth of a hydrocarbonaceous layer on the catalyst surface.[30] In addition, there is less weakly bound hydrogen available at low temperatures (higher temperatures facilitate increased rates of $H_2$ addition) causing an accumulation of carbon species on the surface of the catalysts that promotes octene desorption. In this case, its readsorption and hence isomerization is also prevented. Fairly stable conversions were reached from 6 h reaction time where the possibility exists of a single layer of carbonaceous material deposited over the catalyst surface causing no further deactivation. This implies that the surface of the catalyst remains accessible for adsorption of incoming reactants. Initially, the unsteady steady state of the catalyst may be due to some in situ metal reduction occurring.

The addition of hydrogen to alkynes is favored at most temperatures. At higher temperatures of 80 °C (Figure 4b), 100 °C (Figure 4c), 120 °C (Figure 4d), and 140 °C (Figure 4e), reaction rates improved and, hence, increased initial octyne conversions are noted with little octene isomerization occurring. In Figure 4e, the fairly high, stable alkyne conversion implies decreased carbon deposition at 140 °C.[31] Also, at high enough temperatures, soft or aliphatic hydrocarbon deposits can be easily removed under a hydrogen atmosphere giving decreased rates of deactivation at 140 °C as opposed to 100 and 120 °C.

According to Delgado et al.,[32] hydrocarbon deposits enhance catalyst selectivity, where two types of sites were proposed to be present on the metal surface. There are sites accessible to all reagents and those which are poisoned and coated by carbonaceous deposits and thus inaccessible. These poisoned sites can interact with neighboring atoms and produce hindered sites that become accessible only to the alkyne and hydrogen, thereby increasing alkene selectivity while decreasing alkyne conversion. Thus, in this study, the carbonaceous species can be regarded as both a poison (in terms of octyne conversion) and promoter (regarding selectivity).

In terms of the types of hydrocarbons deposited, at higher temperatures, carbonaceous materials are graphite-like in structure, while carbonaceous materials at low temperatures have soluble and insoluble components. These were confirmed by thermogravimetric analysis−differential scanning calorimetry (TGA−DSC) and are discussed later. Green oil forms as a result of a coupling−hydrogenation mechanism, which is accompanied by polymerization and hydrogenation to form heavier compounds according to eq 1[33]

$$C_8H_{14} + C_8H_{14} \rightarrow C_{16}H_{28} + H_2 \rightarrow C_{16}H_{29} + \frac{1}{2}H_2 \rightarrow C_{16}H_{30} \quad (1)$$



https://doi.org/10.1021/acsomega.1c05231
ACS Omega 2022, 7, 4026−4040

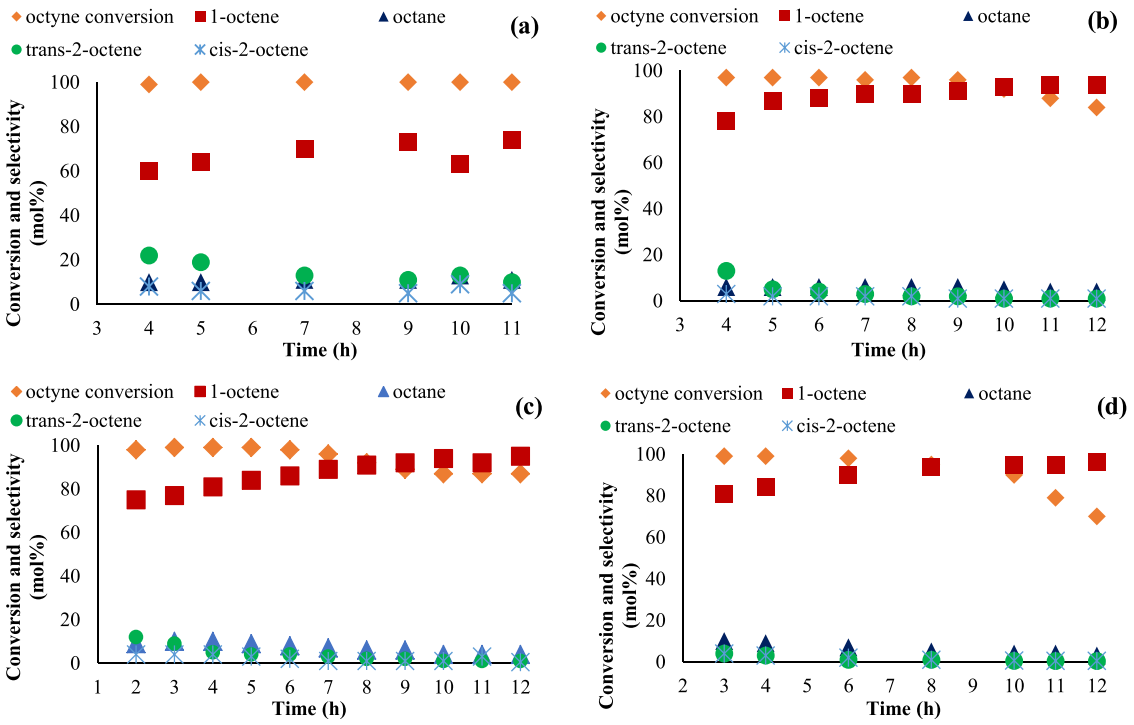


**Figure 5.** Conversion of octyne and selectivity to 1-octene, octane, *cis*-2-octene, and *trans*-2-octene over $5Ag/Al_2O_3$, LHSV: (a) 9 $h^{-1}$, (b) 18 $h^{-1}$, (c) 27 $h^{-1}$, and (d) 36 $h^{-1}$. Reaction conditions: Pressure: 50 bar, temperature: 140 °C, octyne/$H_2$ ratio: 1:1.5, feed: 2 wt % octyne in hexane. The standard deviation for values at 12 h is ±1.5 mol %.

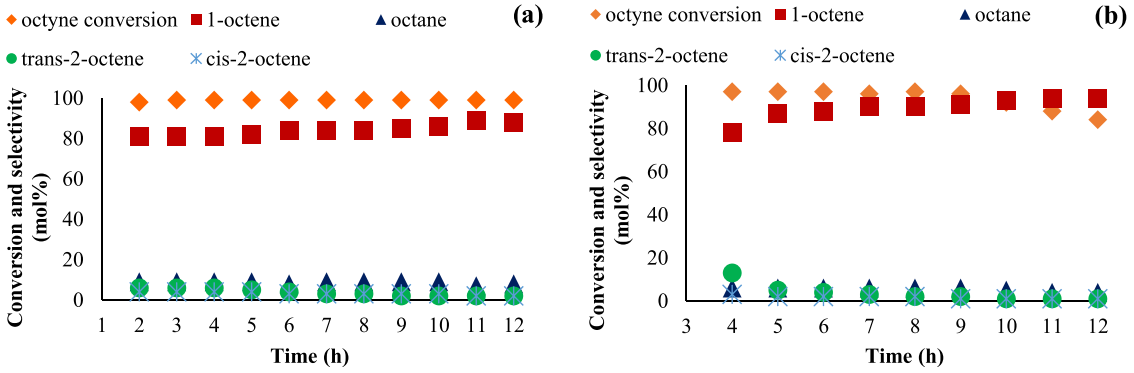


**Figure 6.** Conversion of octyne and selectivity to 1-octene, octane, *cis*-2-octene, and *trans*-2-octene over $5Ag/Al_2O_3$ and pressures of (a) 30 bar and (b) 50 bar. Reaction conditions: Temperature: 140 °C, LHSV: 18 $h^{-1}$, octyne/$H_2$ ratio: 1:1.5, feed: 2 wt % octyne in hexane. The standard deviation for values at 12 h is ±0.5 mol %.

Since the catalyst showed improved stability at 140 °C and a further temperature increase could impede the selectivity to 1-octene by promoting sequential hydrogenation reactions to produce more octane, this temperature was chosen for further investigation on the effects of space velocities, pressure, and Ag loading.

*2.2.2. Liquid Hourly Space Velocity.* Hydrogenation of octene commences immediately after complete consumption of the octyne, and therefore the shortest time required to ensure almost complete binding of the octyne to the catalyst surface is required.[34] Decreasing the space velocity increases the feed residence time and thus decreases the 1-octene selectivity as seen in Figure 5a. The increased interaction between the octyne (and octene) and Ag results in easier readsorption of formed octene on accessible sites, and therefore the sequential hydrogenation to octane becomes easy, as does the formation of isomeric octenes (Figure 5a).

When the space velocity was increased from 9 to 18, 27, and 36 $h^{-1}$ (Figure 5b–d), the selectivity to 1-octene significantly increased and continued to increase during the 12 h time-on-stream. At an LHSV of 27 $h^{-1}$, the catalyst was stable for 6 h on-stream giving full conversion in this time (with some initial overhydrogenation and isomerization occurring), after which a decline in activity was observed (Figure 5c).

1-Octyne conversion began to decrease quite rapidly after 10 h at a liquid hourly space velocity of 36 $h^{-1}$. Reactions run at a high space velocity usually tend to decrease the lifetime of the catalyst.[35] The decreased conversion, influenced by the initial carbon laydown, is attributed to a minimal effective surface concentration of the reactants due to a decreased contact time, and hence, residence time, which ultimately reduced the interaction between the active Ag sites and the reactant feed. At these space velocities, isomeric octenes selectivity significantly decreased by decreasing the overall surface



https://doi.org/10.1021/acsomega.1c05231
ACS Omega 2022, 7, 4026−4040

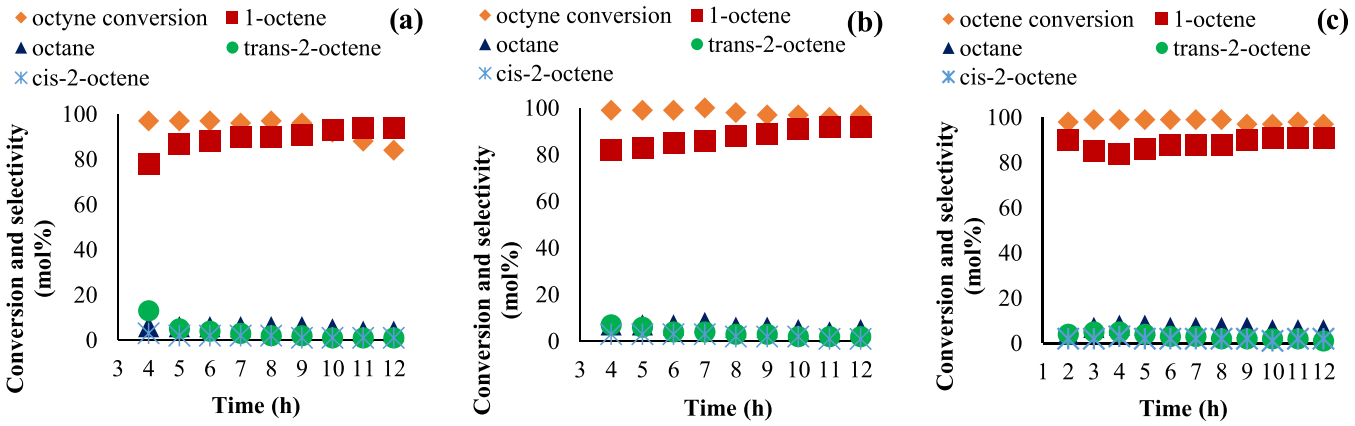


**Figure 7.** Conversion of octyne and selectivity toward 1-octene, octane, *cis*-2-octene, and *trans*-2-octene over $5Ag/Al_2O_3$ and octyne/$H_2$ ratios of (a) 1:1.5, (b) 1:2, and (c) 1:3.5. Reaction conditions: Pressure: 50 bar, temperature: 140 °C, LHSV: 18 $h^{-1}$, octyne/$H_2$ ratio: 1:1.5, feed: 2 wt % octyne in hexane. The standard deviation for values at 12 h is ±1 mol %.

interactions. In contrast, the octene isomers formed at an LHSV of 9 $h^{-1}$ were maximized due to the formation and readsorption of the octene on available Ag sites since initial alkyne−Ag surface interactions were enhanced by longer residence times. The conversion and selectivity profile at 18 $h^{-1}$ showed good selectivity to 1-octene and minimal formation of overhydrogenation and isomerization products with slight deactivation, and hence, this LHSV was applied for further reactions.

*2.2.3. Pressure.* At a 50 bar hydrogen pressure (Figure 6b), the initial full octyne conversion shows that the rate of hydrogen addition is fast, but due to the stronger adsorption of octyne over hydrogen, the surface starts to become covered with the reactant over time, leaving fewer adsorption sites available for hydrogen. These species begin to accumulate and thus eventually start to deactivate the catalyst from 10 h on-stream. Typically, hydrogen pressures used in industry are between 15 and 35 bar, and usually high pressures are associated with high surface coverages.[36] Following this norm, a decrease in the hydrogen pressure causes a decrease in the total hydrogenation of octyne as a result of the reduced surface concentration of hydrogen. With this, the initial carbon layer deposited may be thicker than at higher pressures due to reduced surface hydrogen species. This reduces the amount of overhydrogenated and isomerized products in the early hours of the reaction (Figure 6a). It has been proposed by Parera et al.[37] that a low hydrogen pressure produces a large amount of coke on the metal and not on the support; however, the stability of this catalyst shows that the carbon deposits are not severe enough to deactivate the catalyst during this time.

*2.2.4. Effect of GHSV.* In theory, increasing the effective surface hydrogen concentration increases the hydrogenation rate. Work done by Larsson et al.[38] revealed that a high enough content of hydrogen could suppress the formation of highly unsaturated species responsible for coking because the rate of hydrogenation of the alkyne is faster when there is a high surface coverage of the active sites by hydrogen. When the surface coverage of hydrogen is low, the half-hydrogenated species (from the addition of a single hydrogen atom) increase. These species can react with other intermediates on the catalyst surface and form coke or coke precursors.

Figure 7a shows that the catalyst at a $H_2$/octyne ratio of 1.5 is unstable due to the low hydrogen content fed. This implies that the rate of addition of hydrogen, which is considered the rate-determining step (RDS) of alkyne hydrogenation,[39] is slower than the rate of adsorption of the octyne over the catalyst surface. According to McCue et al., oligomer chain growth is promoted at a low hydrogen concentration.[36]

Figure 7c shows that 3.5 equiv of hydrogen to octyne gives a rate of addition of hydrogen to octyne that is faster than the rate at lower hydrogen content (in agreement with the literature).[40] Thus, it shows better 1-octyne conversions and 1-octene selectivities than were seen at a $H_2$/octyne ratio of 2 (Figure 7b). Despite the increased rates of hydrogenation, carbonaceous deposits still form over the active Ag sites because the dissociation of hydrogen by silver is still weak and therefore once octyne is adsorbed over the catalyst surface, the immediate hydrogen addition (to form octene) is not compensated by the rate at which hydrogen is dissociated by the metal to repopulate the catalyst surface. This leaves empty sites available for octyne coverage and thus coke formation.

In other reports, increasing the $H_2$ content relative to the substrate was seen to lower alkene selectivity, first by removing carbides that would hinder readsorption of 1-octene by mass transfer effects and second, by promoting the formation of a hydride phase, which readily produces alkanes.[41] In this study, the stability of the catalysts at high $H_2$ concentrations (Figure 7b,c) suggests that by light carbon laydown occurring on the surface of the catalysts, by steric hindrance, a steady state in the conversion of octyne is maintained with time, provided there is an equilibrium between the rate of hydrogen addition and the rate of octene desorption from the catalyst surface.

In all cases (Figure 7a−c) and irrespective of hydrogen coverage influencing hydrogenation rates (hydrogen is weakly adsorbed over the catalyst surface compared to alkynes),[10] once octyne is adsorbed over the Ag surface, it is immediately hydrogenated to form octene. Initially, the surface of the catalyst is essentially carbon-free, where the role of hydrogen is also to preserve the clean surface of the catalyst.[42] The carbon layer builds with time and may form multilayers depending on the amount of hydrogen fed. Hence, initially, less 1-octene is observed due to readsorption of 1-octene onto "uncovered" sites, where octane forms. As the layer of carbon accumulates on the catalyst surface, the formed octene (having a lower heat of adsorption compared to octyne) desorbs quickly from the surface with minimal readsorption and, therefore, at full octyne conversion, increasing selectivities are seen to 1-octene with time. In this instance, the propensity of 1-octene to further



https://doi.org/10.1021/acsomega.1c05231
ACS Omega 2022, 7, 4026−4040

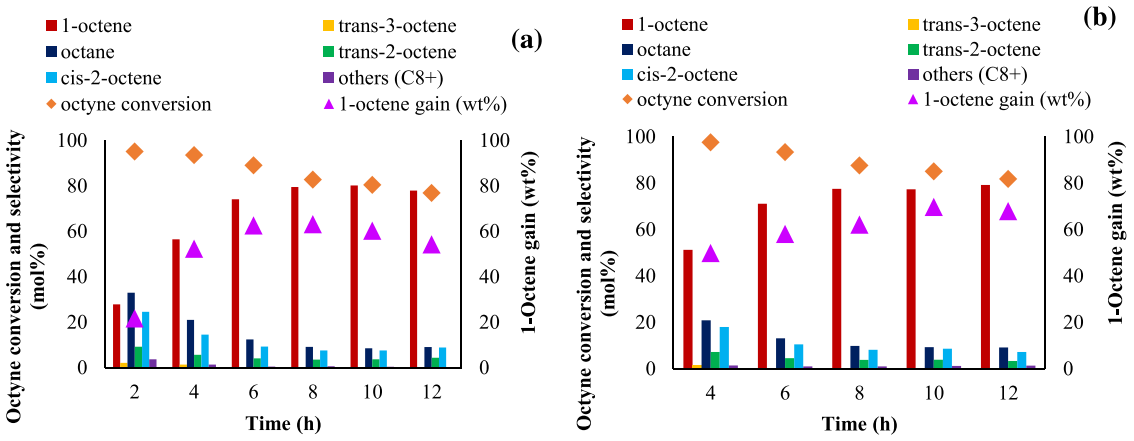


**Figure 8.** Conversion of octyne and selectivity toward 1-octene, octane, *cis*-2-octene, and *trans*-2-octene over (a) $2Ag/Al_2O_3$ and (b) $10Ag/Al_2O_3$. Reaction conditions: Pressure: 30 bar, temperature: 140 °C, LHSV: 18 $h^{-1}$, octyne/$H_2$ ratio: 1:3.5, feed: 2 wt % octyne, 10 wt % octene in hexane. The standard deviation for values at 12 h is ±0.5 mol %.

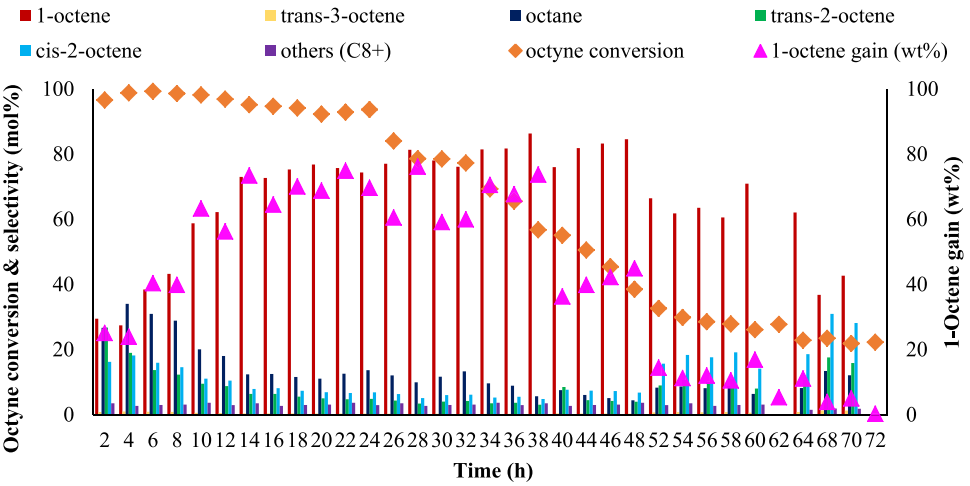


**Figure 9.** Conversion of octyne and selectivity toward 1-octene, octane, *cis*-2-octene, and *trans*-2-octene over $5Ag/Al_2O_3$. Reaction conditions: LHSV: 18 $h^{-1}$, pressure: 30 bar, octyne/$H_2$ ratio: 1:3.5, temperature: 140 °C, feed: 2 wt % octyne, 10 wt % octene in hexane.

hydrogenate to octane (due to a diffusion barrier caused by the layer of carbon species initially forming) is limited.

**2.3. Competitive Hydrogenation of Octyne vs Octene.** *2.3.1. Ag Weight Loading.* The effect of silver weight loading on the extent of coverage of $\gamma$-$Al_2O_3$ by the active metal was investigated. There is a clear indication that with a low surface coverage of the carrier by silver ($2Ag/Al_2O_3$, Figure 8a), there are more exposed acidic (Lewis and Brønsted) sites and, thus, the extent to which the deactivation of the catalyst occurs is faster, as opposed to a catalyst with a higher silver loading ($10Ag/Al_2O_3$, Figure 8b), which covers more of the support and, hence, shows a decreased rate of formation of carbon deposits causing catalyst deactivation. In both cases (Figure 8a,b), initially, the catalyst surfaces are essentially carbon-free and, hence, give full conversion. Since there are free sites, which become available after complete consumption of the octyne, to readsorb octene (after its formation), some octene is hydrogenated to octane. Furthermore, isomeric octenes are also initially formed, since some of the formed octene readsorbs onto a different active site for isomerization. As the layers of carbon material build, the 1-octene selectivity (based on the gain of 1-octene) improves due to diffusion limitations, making the readsorbtion of octene difficult. However, the surface of the catalyst now becomes deactivated with time.

This was not observed over the $5Ag/Al_2O_3$ catalyst (discussed in the next section, Figure 9), which seemed to provide the best balance between metal particle size, metal–support coverage, and surface interaction, as well as the best dispersion from chemisorption studies (Table S1), justifying its choice as a baseline catalyst for the noncompetitive reactions. This catalyst was also used to investigate long-term catalyst stability, for up to 72 h. IPA-TPD measurements of $5Ag/Al_2O_3$ revealed a few Brønsted acid sites (0.150 mmol/g) on the surface, implying that byproduct selectivity should be low and this result is confirmed by the stability test, discussed in the next section.

*2.3.2. Stability Test on $5Ag/Al_2O_3$.* From the reaction conditions explored in the noncompetitive hydrogenation reactions, the chosen conditions of 30 bar pressure, 140 °C temperature, 18 $h^{-1}$ LHSV, and 1:3.5 octyne/$H_2$ ratio were used with the competitive feed comprising 2 wt % octyne and 10 wt % octene in hexane. The chosen pressure and space velocities gave minimal oligomer formation (from the GC traces) and, from a report by Bos and Westerterp,[43] very high hydrogen pressures typically favor the production of octane by direct hydrogenation of octyne. This possibility was ruled out



https://doi.org/10.1021/acsomega.1c05231
ACS Omega 2022, 7, 4026−4040

**Scheme 2. Mechanism for the Hydrogenation of Octyne, Showing Multiple Pathways and Formed Intermediates**

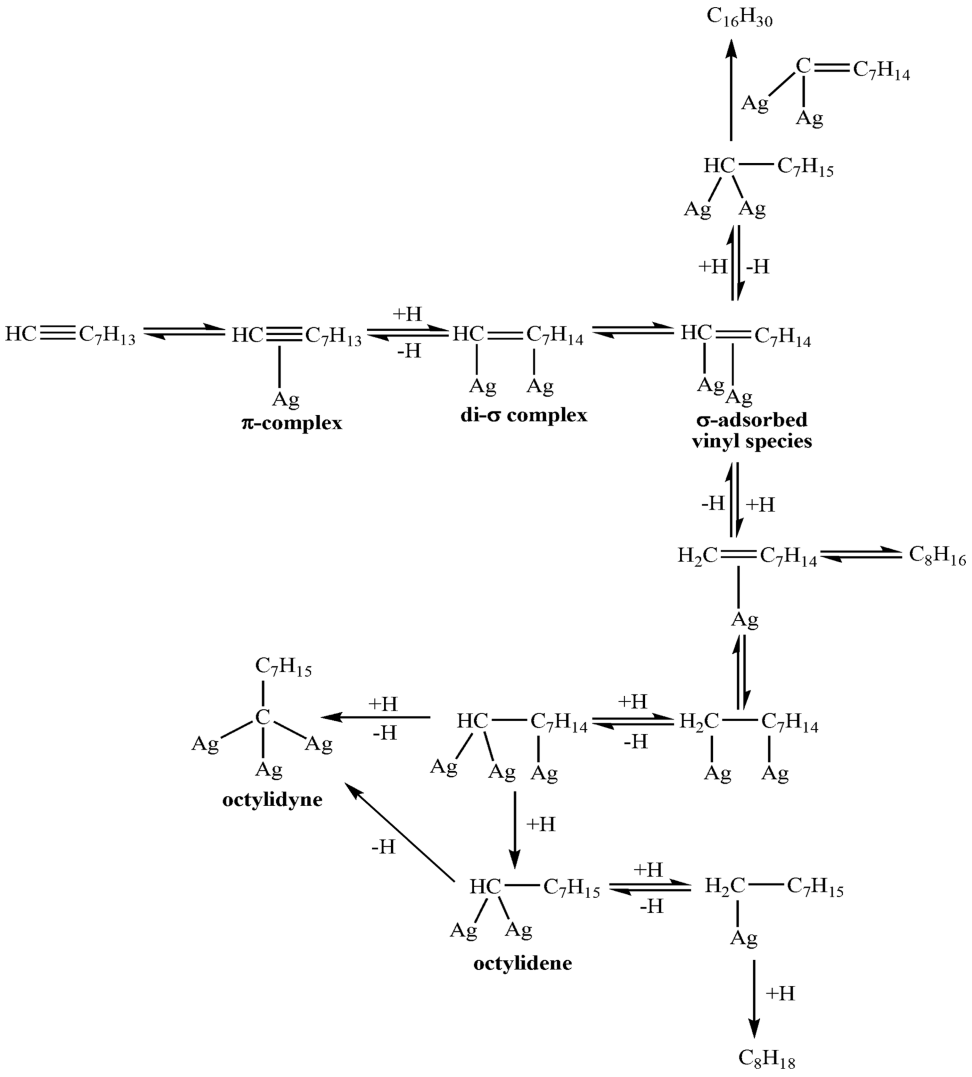


in this work since bands due to strongly adsorbed vinylidene species (usually occurring around 1430 $cm^{-1}$) were not seen in the IR spectra of the used catalysts (Figures S3−S5). These vinylidene species are reported to be responsible for directly producing octane from octyne.[7]

In the competitive feed system, stronger adsorption of 1-octyne over 1-octene improves selectivity up to a point, as seen in Figure 9. Octyne is generally less thermodynamically stable than 1-octene due to their nature of bonding and thus adsorbs strongly on the catalyst surface. Octene hydrogenation is inhibited in the presence of octyne but can occur spontaneously as shown in the previous section. Alkynes can adsorb and hydrogenate on both flat and terrace surfaces (low-coordination sites), but alkenes react faster on flat sites as a result of steric hindrance to adsorption on terraces.[41]

Other formed products ("others") include a mixture of internal octenes, octane, and minor quantities of di-octenes and aromatics. Many studies have proposed that blockage of active surface sites for the adsorption of alkenes (caused by the alkyne) makes the system selective to the alkene. The carbon-free catalyst surface gives 100% 1-octyne conversion because the initial adsorbed reactants are slowly replaced by a new layer of adsorbates (through hydrogen addition), forming octenes and possibly octane.

The results also show that over time, there is no 1-octene conversion due to selective poisoning, where the ability of the catalyst to hydrogenate octene remains low, while at the same time hydrogenating the octyne. Also, the decreasing octane and internal octene selectivity over the 72 h time-on-stream shows that the slow carbon laydown prevents octene readsorption and, hence, further hydrogenation or isomerization.

Two stages of deactivation can be noted. The first occurs rapidly between 24 and 54 h on-stream with increasing 1-octene gain. Over this time, the relative light carbon deposits on or in the vicinity of the Ag surface polymerize and accumulate as heavy carbon material. As this layer of carbon builds up past 54 h on-stream (stage 2 deactivation), the surface of the catalyst now becomes completely covered or blocked and thus octyne conversion levels off due to insufficient availability of active sites. At this stage, a slower deactivation rate is observed. The buildup of coke deposits and the resultant reduction in active surface area limit the diffusion and thus adsorption of octyne. Thus, the octene formed increases until 48 h on-stream, as the metal-carbon phase weakens the hydrogen adsorption by decreasing its chemisorption energy and hence its coverage, thus promoting faster octene desorption.[44] The selectivity to 1-octene then decreases


https://doi.org/10.1021/acsomega.1c05231
ACS Omega 2022, 7, 4026−4040

over time when octyne and hydrogen can no longer diffuse through the thick carbon film, which leads to a hydrogen-starved surface. Also, at this stage, there is a higher steady-state coverage of strongly bound deposits that block large portions of the active silver metal sites. Thus, the alumina provides the active sites to catalyze the isomerization of any formed and readsorbed octenes; hence, octene isomers are increasingly produced beyond 54 h on-stream.

Carbon species can have a promoting effect and thus prove beneficial by poisoning nonselective active sites. Also, when a carbide phase forms, octene selectivity increases since the coke destabilizes the octene adsorbed on the surface and it desorbs before further hydrogenation occurs. This effect is seen during the first 24 h of reaction where the 1-octene selectivity increases from 30% initially to 80% after 24 h. If subsurface carbides are considered, then this leads to a decrease in the activation barriers of octyne and octene and increases the activation barriers of C−C coupling, thus hindering oligomerization and raising octene selectivity.[41]

In the last stage of the deactivation (beyond 48 h on-stream), there is increased *cis*-2-octene formation because the 1-octene formed isomerizes by returning to an acidic site on the surface. STEM-EDX characterization of the used catalyst gave insight into a sintering mechanism occurring in parallel to catalyst deactivation caused by coking. Particle sizes appeared larger in the used catalyst (31.9 nm compared to 11.5 nm for the fresh catalyst) and this correlates to a dispersion effect in that larger agglomerates of silver expose more acidic sites of alumina for side reactions. Hence, in the second stage of deactivation, Figure 9 (24−54 h), it is likely that the large agglomerates are deactivated by the coke coating the catalyst surface. At this stage, the olefin selectivity obeys the literature trend:[45] 1-octene > *cis*-2-octene > *trans*-2-octene > *trans*-3-octene > *trans*-4-octene; *cis*-2-octene is dominantly formed in terms of internal octenes.

**2.4. Mechanistic Considerations.** The heats of adsorption of alkynes are larger (−14 kJ/mol) compared to alkenes and thus readily adsorb on the catalyst surface.[39] Zhang et al. report that one surface atom adsorbs one hydrogen atom.[46] Alkynes adsorb as strong di-$\sigma$ bonds (on two neighboring metal atoms) or weak $\pi$-bonds (on one metal atom), where the $\pi$-adsorbed species leads to the selective hydrogenation to alkenes, while the former give alkanes.[47]

Pachulski et al. proposed that two active sites are involved in the hydrogenation of alkynes (Scheme 2).[39] Octene forms on the first site by the reaction of molecular adsorbed octyne with two dissociatively adsorbed hydrogen atoms under participation of a vinylidene species that is adsorbed on the catalyst surface. Initially, the octyne adsorbs on the catalyst surface as a $\pi$-complex, which can then be converted to a di-$\sigma$-adsorbed species. The vinylidene surface intermediate forms by the addition of one hydrogen atom to the chemisorbed octyne. This species is considered key in the hydrogenation of octyne to octene. On the same site, two vinyl species and hydrogen react to give octenes. Octene is associatively adsorbed on a second site and converted to octane by reaction with dissociatively adsorbed hydrogen atoms. Octene can also adsorb on the first site, but the conversion to octane predominantly occurs on the second. Dissociatively adsorbed octyne and vinylidene species are said to be responsible for oligomerization reactions, which is supported by the results of the stability experiment carried out in this study.[34] The rate-determining step in the hydrogenation of octyne to octene is the addition of the first hydrogen atom, while the addition of the second hydrogen atom is the RDS for the hydrogenation of octene to octane.

**2.5. Deactivation by Coking and Sintering.** *2.5.1. TGA−DSC.* Thermogravimetric analyses were used to quantify the amount of carbon deposits on the surfaces of the used catalysts, Figure S6. There is a significant amount of carbon deposition on the surface of the catalysts. In general, increasing the amount of dispersed metal on a catalyst causes less coke formation because more acidic sites on the support are covered. TGA provides information on the specific hydrocarbon species deposited, with soft (aliphatic) hydrocarbons being typically found in the 200−400 °C region, while hard (graphite-like) hydrocarbons are represented by a weight loss in the 400−600 °C region.[48]

From Table 2, peaks in the range of 100−120 °C are due to the loss of water within the pores of the catalyst. This loss ranges from 3 to 4.5 wt % across the different weight loadings of silver. The content of aliphatic hydrocarbon deposition over all $Ag/Al_2O_3$ catalysts is significantly lower than the amount of hard coke deposited. The accumulated carbonaceous material can be further identified by the Raman scattering effect, which is dependent on the polarizability of the species and can thus be used to indicate the degree of graphicity of a carbon network (Figure S7). The two peaks are representative of D and G bands (1382 and 1581 $cm^{-1}$, respectively) which are related to the deposition of amorphous graphite (disordered) and hard coke, respectively.[49] In addition, the majority of carbonaceous material was deposited on the acidic part of the catalyst (alumina) after initial deposition over the metal[50] as confirmed by the TPO-MS results of the $10Ag/Al_2O_3$ catalyst (Figure S8). Coke deposition occurs on the metal first followed by deposition on the acidic alumina (Figure S8).

**Table 2. TGA Data for All Used $Ag/Al_2O_3$ Catalysts**

| catalyst | moisture (%) 100−120 °C | aliphatic species (%) 200−400 °C | graphite species (%) 400−600 °C | total weight loss (%) |
|---|---|---|---|---|
| $2Ag/Al_2O_3$[a] | 3.5 | 3 | 4 | 10.5 |
| $5Ag/Al_2O_3$[b] | 3 | 1.5 | 10.5 | 15 |
| $10Ag/Al_2O_3$[a] | 4.5 | 2 | 8 | 14.5 |

[a]Reaction time: 12 h. [b]Reaction time: 72 h.

*2.5.2. STEM-EDX.* From Figure 10, analysis of the used $5Ag/Al_2O_3$ (Figure 10a−c) by STEM-EDX shows the presence of a sintering mechanism. Figure 10b,c shows the silver and alumina maps, respectively, with the bulk of the catalyst being alumina (Figure 10c). In the silver map, due to clustering of silver occurring in specific regions, intense bright spots are seen in the BSE image (Figure 10a). The extent of agglomeration of silver is clear from a comparison of the particle size distribution graphs between the fresh and used $5Ag/Al_2O_3$. The average particle size in the fresh catalyst was 11.5 nm (Figure 2e) with good dispersion of silver over the alumina support.

From the map combining silver and alumina (Figure 10d), it can be seen that the dispersion of the used $5Ag/Al_2O_3$ is still reasonably good, which can be correlated with the average particle size of 31.9 nm (Figure 10f). This confirms that sintering occurs during the catalysis. Figure 10e shows



https://doi.org/10.1021/acsomega.1c05231
ACS Omega 2022, 7, 4026−4040

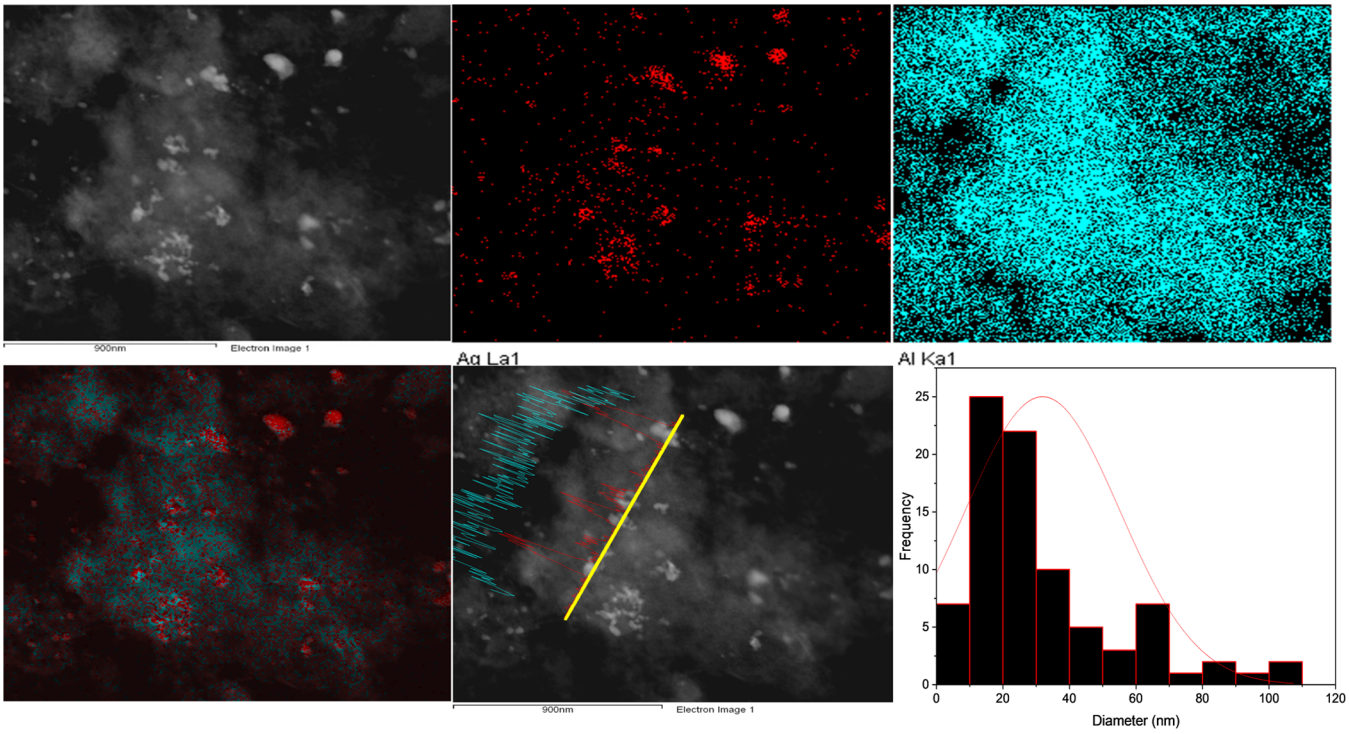


**Figure 10.** STEM-EDX images for the used 5Ag/$Al_2O_3$ showing (a) dark-field image, (b) silver map, (c) aluminum map, (d) silver and aluminum map, (e) line scan image, and (f) particle size distribution graph after reaction using 2% octyne and 10% octene in hexane.

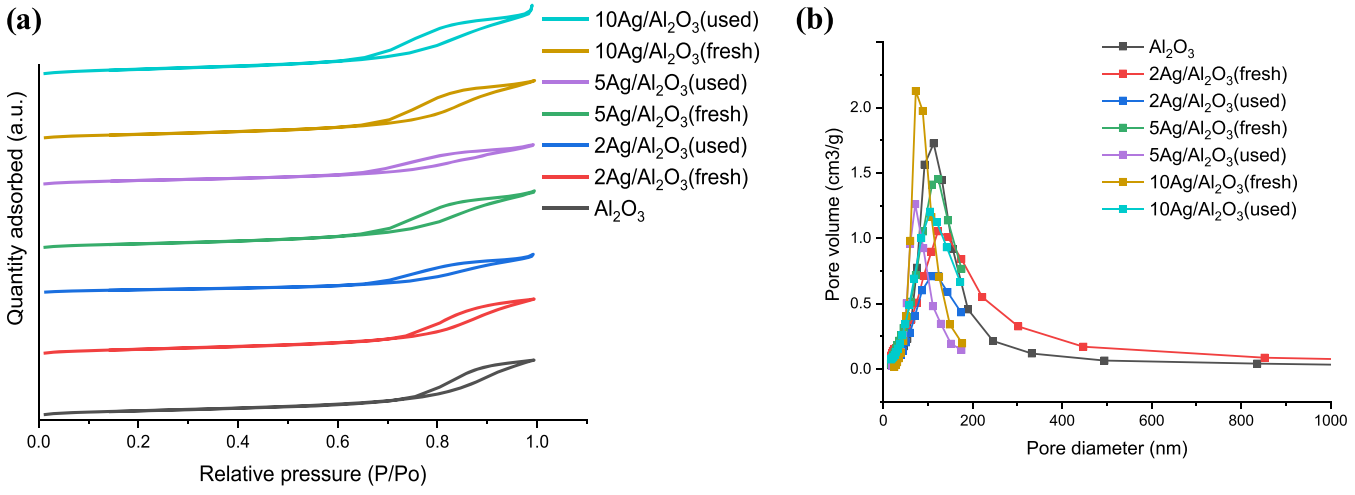


**Figure 11.** BET measurements of fresh and used Ag/$Al_2O_3$ catalysts showing (a) $N_2$ adsorption/desorption isotherms and (b) pore size distribution.

enrichment of silver across the region of the line scan, further emphasizing the dispersion of silver over the carrier. This can be attributed to carbon deposition as a layer over and surrounding the original small crystallites of silver, which prevents rapid sintering during the reaction. Silver agglomerates were also observed for the used 2Ag/$Al_2O_3$ and 10Ag/$Al_2O_3$ catalysts (Figures S9 and S10) with the least amount of agglomeration and clustering occurring in the 2Ag/$Al_2O_3$ catalyst, while the most intense coalescence of silver atoms was seen with the 10Ag/$Al_2O_3$ sample.

**2.6. Further Used Catalyst Characterization.** *2.6.1. $N_2$ Physisorption Measurements.* Brunauer–Emmett–Teller (BET) surface area analyses of the fresh and used silver catalysts showed significant changes within the network of pores in each catalyst. From Figure 11a, all catalysts exhibit Type IV isotherms with H3 hysteresis loops. This shows that all catalyst pores are ink-bottle-shaped with a narrow neck and wider cavity. There are marked changes to the pore shapes of the used catalysts, as shown by the nitrogen adsorption/desorption isotherms. These changes are noted by narrower isotherms exhibited by the used catalysts compared to those of the fresh samples suggesting pore filling by carbonaceous material.

All isotherms are characteristic of mesopore materials having pore sizes typically in the range of 2–50 nm. Figure 11b illustrates pore size distribution plots for each fresh and used catalyst. The used 2Ag/$Al_2O_3$ catalyst showed a pore size distribution in the range 5–20 nm (being the largest among



https://doi.org/10.1021/acsomega.1c05231
ACS Omega 2022, 7, 4026–4040

the series of catalysts), while the used 5Ag/$Al_2O_3$ catalyst showed the narrowest pore size distribution (5−10 nm). The pore size distribution measurements of the used catalysts confirm that the pore entrances are being blocked by the buildup of carbon material, hence giving a narrow pore size distribution curve in the case of the used 5Ag/$Al_2O_3$ catalyst.

The surface areas of the fresh catalysts were seen to decrease with the amount of silver loaded (Table 3). This decrease is attributed to the deposition of silver metal within the pores of the catalysts. All used catalysts show a significantly lower surface area compared to the fresh catalysts due to the aforementioned deposition of carbon occurring on the surface of the catalysts. The extent of this was greater over the 5Ag/$Al_2O_3$ catalyst due to the prolonged reaction time, which allowed for ample accumulation of aliphatic and graphite-like hydrocarbons to block the pores and pore entrances of the catalyst and cause deactivation. For this reason, the pore volume of the catalyst drastically decreases at the end of the reaction compared to the value at the onset (Table 3). The results also explain why within 12 h on-stream, the 2Ag/$Al_2O_3$ catalyst deactivates the fastest (shown by a drastic decrease in surface area from fresh to used catalyst) as the low Ag loading leaves more exposed alumina sites. This means that the carbon material will accumulate faster over the surface of the catalyst compared to the 10Ag/$Al_2O_3$ catalyst, which has a higher Ag loading with a few exposed alumina sites to cause a rapid deactivation of the catalyst.

**Table 3. Surface Properties of the Fresh and Used Ag/$Al_2O_3$ Catalysts**

| catalyst | surface area ($m^2$/g) | pore volume ($cm^3$/g) | pore diameter (nm) |
|---|---|---|---|
| $Al_2O_3$ | 255 ± 3 | 0.72 | 10.0 |
| 2Ag/$Al_2O_3$ (fresh) | 253 ± 0.5 | 0.70 | 9.4 |
| 2Ag/$Al_2O_3$ (used)[a] | 141 ± 1 | 0.39 | 7.8 |
| 5Ag/$Al_2O_3$ (fresh) | 234 ± 1.5 | 0.63 | 7.6 |
| 5Ag/$Al_2O_3$ (used)[b] | 177 ± 3 | 0.42 | 7.0 |
| 10Ag/$Al_2O_3$ (fresh) | 229 ± 2 | 0.66 | 7.8 |
| 10Ag/$Al_2O_3$ (used)[a] | 211 ± 1 | 0.65 | 7.2 |

[a]Reaction time: 12 h. [b]Reaction time: 72 h.

*2.6.2. ICP-OES.* The extent to which the catalytic activity was seen to decline at the end of each reaction prompted the investigation into three different types of deactivation mechanisms, namely, leaching, sintering, and coking. From the actual weight loadings of the spent catalysts compared to those of the fresh (Table 4), where each result was obtained in triplicate, there are at most negligible amounts of silver lost at the end of each reaction. This means that a decline in catalytic activity caused by leaching of the active metal can be ruled out as a possible deactivation mechanism.

**Table 4. Actual Weight Loadings of Deactivated Catalysts Obtained from ICP-OES Analysis**

| catalyst | fresh | used |
|---|---|---|
| 2Ag/$Al_2O_3$[a] | 2.28 ± 0.22 | 1.92 ± 0.07 |
| 5Ag/$Al_2O_3$[b] | 4.87 ± 0.08 | 4.67 ± 0.23 |
| 10Ag/$Al_2O_3$[a] | 10.49 ± 0.67 | 9.62 ± 1.55 |

[a]Reaction time: 12 h. [b]Reaction time: 72 h.

## 3. SUMMARY AND CONCLUSIONS

It was shown from microscopy analyses and temperature-programmed techniques that the 5Ag/$Al_2O_3$ catalyst had good dispersion (7.9%) and degree of reduction (88%) of silver compared to the other tested catalysts. The average particle size ranged from 4 to 21 nm. As a baseline catalyst in the noncompetitive hydrogenation of 1-octyne, high conversion and 1-octene selectivity were obtained under the following conditions: LHSV: 18 $h^{-1}$, pressure: 30 bar, octyne/$H_2$ ratio: 1:3.5, temperature: 140 °C. Increasing the content of surface hydrogen available and decreasing the residence time for the incoming reactants (i.e., higher pressures and GHSVs and lower LHSVs) provided a more stable catalyst for longer reaction periods with less overhydrogenation and isomerization products.

Mimicking these conditions in the competitive hydrogenation reaction over the 2Ag/$Al_2O_3$ and 10Ag/$Al_2O_3$ catalysts revealed a steady decline in activity over 12 h with the deactivation rate being faster over the 2Ag/$Al_2O_3$ catalyst. In contrast, the 5Ag/$Al_2O_3$ catalyst showed high stable activity over this time period. Exposed alumina sites (higher on the 2Ag/$Al_2O_3$ catalyst than the 10Ag/$Al_2O_3$ catalyst) were confirmed by microscopy and dispersion measurements. IPA-TPD studies on the fresh 5Ag/$Al_2O_3$ catalyst showed a few Brønsted acid sites (0.150 mmol/g) available for side reactions. Thermogravimetric analyses and Raman studies revealed the deposition of soft and hard coke over the catalyst surface as well as at pore entrances (shown by BET measurements) during 72 h on-stream. The catalysis also showed that with increasing carbide formation, 1-octene gain increased steadily. Leaching was ruled out as a deactivation mechanism. From STEM-EDX techniques, metal sintering was shown by increased particles sizes in used (31.9 nm) vs fresh (11.5 nm) catalysts.

## 4. EXPERIMENTAL SECTION

The catalysts consisting of 2, 5, and 10 wt % Ag on $Al_2O_3$ were prepared by deposition precipitation with silver nitrate hexahydrate (Sigma-Aldrich, 99.9%) and γ-alumina (Merck, 99%) as the precursor salt and carrier, respectively. The pH of all support solutions was adjusted to 10 with 25% ammonia solution followed by dropwise addition of the metal solution. All catalysts were dried over 8 h using a rotary evaporator at 70 °C under reduced pressure. Samples were then oven-dried overnight at 110 °C prior to a calcination step at 500 °C for 12 h. All catalysts were activated under pure hydrogen at 160 °C for 12 h at 40 mL/min.

Pulse chemisorption TPD-MS studies were carried out on an AutoChem 2920 instrument coupled with a Cirrus Mass Spectrometer (MKS Instruments) to investigate the Brønsted acidic sites present on the catalysts analyzed. The catalyst (∼70 mg) temperature was ramped from RT to 160 °C at 10 °C/min in a flow of helium (30 mL/min) and pretreated at this temperature for 2 h. Thereafter, the sample was cooled to 100 °C with helium (30 mL/min) for the pulse chemisorption measurements, followed by pulsing 30 times with 1 mL of IPA in a flow of helium at 3-min intervals. The temperature was then raised at 10 °C/min to 500 °C under 30 mL/min helium for the desorption analysis, where mass spectrometry was used



https://doi.org/10.1021/acsomega.1c05231
ACS Omega 2022, 7, 4026−4040

to distinguish the desorbing *n*-propylamine ($m/z$ = 44), propene ($m/z$ = 41), and ammonia ($m/z$ = 17) species, of which the amount of propylene species desorbed was quantified for the amount of Brønsted acidic sites present.

The catalyst (90 mg) temperature was ramped from RT to 160 °C at 10 °C/min in a flow of helium (30 mL/min) for 2 h in a Micromeritics 2920 instrument. At this temperature, the catalyst was activated under pure hydrogen at 50 mL/min for 4 h. Thereafter, 5% $O_2$/He gas was passed over the sample at a flow rate of 20 mL/min and held for 1 h. The catalyst was then heated from 30 °C to 700 °C at 10 °C/min.

Specific surface areas, pore volumes, and pore size distribution analyses were obtained using a Micromeritics TriStar II 3020 surface area and porosity instrument, where the temperature was maintained at −195 °C. Approximately 100 mg of each catalyst was degassed under nitrogen, first at 90 °C for 1 h to remove physisorbed moisture and then at 200 °C for 12 h. All measurements were conducted in triplicate to ensure reproducibility.

A spatula tip of the sample was added to an Eppendorf vial and suspended in acetone. The mixture was sonicated for 5 min to disperse the catalyst. The sample was then coated onto holey carbon grids and placed into a Jeol 1010 TEM instrument and analyzed using the Megaview III software imaging system at an operating voltage of 200 kV.

Backscattered electron (BSE) imaging and energy-dispersive X-ray spectroscopy (EDS) analyses were carried out on a Zeiss EVO 40 instrument equipped with a tungsten filament. BSE imaging and EDS mapping were done at an accelerating voltage of 20 kV at a probe current of 1.5 nA. The filament current was kept constant at 2.403 A. EDS analyses were performed using a Bruker XFlash SDD detector using Bruker Esprit software. The samples were cured with Akasel epoxy resin and Akasel cure, which were then polished using diamond paste and coated with carbon. The "detection" of Fe was most probably a result of overlapping or very close signals detected in the EDX spectrum.[51]

Hydrogen-temperature-programmed reduction (TPR) studies were conducted using a Micromeritics Autochem II Chemisorption Analyzer 2920 instrument using approximately 50 mg of each catalyst. The sample was first pretreated at 100 °C under a stream of He (30 mL/min) for 60 min; thereafter, the temperature was decreased to 40 °C under the same inert conditions. The reduction experiments were carried out using 5 vol% $H_2$/Ar at a flow rate of 50 mL/min and a temperature ramp from 40 °C to 800 °C at 10 °C/min.

Hydrogen chemisorption experiments were carried out using a Micromeritics ASAP 2020 instrument and used to determine the metal dispersion and crystallite size. Prior to analysis, approximately 250 mg of sample was degassed under a flow of N2 from RT to 200 °C (held for 12 h) during which the sample was first held at 90 °C for 1 h to remove physisorbed moisture prior to increasing to the final temperature of 200 °C. The sample was then packed between two layers of quartz wool in a quartz U-tube. The analysis pretreatment involved reducing with $H_2$ at 160 °C for 4 h followed by analysis at 140 °C with hydrogen at a 1:0.5 $H_2$-metal stoichiometry. Points at 3, 6, 9, 12, 15, 18, 21, 100, 150, 200, 250, 300, 350, and 400 mmHg were taken on the pressure table. The hydrogen chemisorption capacity was determined by extrapolation of the hydrogen uptake to zero pressure.

The amount of silver present in each sample was determined by ICP-OES using an Optima 5300 DV PerkinElmer Optical Emission Spectrometer. Accurately weighed samples (50 mg) were digested on a hotplate in 10 mL of nitric acid, followed by filtration through a 0.45 $\mu$m filter. ICP standards ranging from 0 to 100 ppm were prepared from a silver stock standard solution of 1000 ppm (Industrial Analytical, RSA). All analyses were carried out in triplicate.

For the TGA−DSC technique, a PE SDTQ600 instrument was used where a small amount of sample was weighed and placed in a sample holder. The analysis involved heating the sample under a stream of air from room temperature to 900 °C at a heating rate of 10 °C/min.

All IR spectra were recorded on a PerkinElmer attenuated total reflectance (ATR) spectrophotometer. The sample was placed on a diamond window and pressurized. All spectra were recorded in the region of 380−4000 $cm^{-1}$ at a resolution of 4 $cm^{-1}$.

All Raman spectroscopy analyses were carried out using a Delta Nu Advantage 532 instrument equipped with a 532 nm laser source (green) and operated by NuSpec software. Laser intensities and the integration time of the scans were varied until each sample gave clear and reproducible spectra. All analyses were carried out at room temperature with the powdered sample loaded in quartz tubes.

Powder X-ray diffraction was carried out using an X-ray diffractometer D8-Advance from Bruker operated in a continuous $\theta-\theta$ scan in locked coupled mode with Cu K$\alpha$ radiation ($\lambda$ = 1.5406 Å). The sample was mounted in the center of the sample holder on a glass slide and leveled up to the correct height. The measurements were run within a $2\theta$ range of 10−90° with a typical step size of 0.034°. A position-sensitive detector, LYNXEYE, was used to record diffraction data at a typical speed of 0.5 sec/step, which is equivalent to an effective time of 92 s/step for a scintillation counter.

A continuous, plug flow fixed-bed reactor was operated for all catalytic work carried out in the liquid phase (Figure S1). The catalyst (2 mL) pellets (300−600 $\mu$m) were diluted in a 1:1 ratio with 24 $\mu$m carborundum and loaded into a 316 stainless steel reactor tube with an inner diameter of 15 mm and length of 325 mm. The catalyst bed was sandwiched between two layers of glass wool, while the remainder of the tube was packed with carborundum and a layer of glass wool at the extreme ends of the reactor tube to prevent particulate matter from entering the product stream. All catalysts were dried under $N_2$ atmosphere at 200 °C for 12 h before blending with hydrogen at 160 °C over 8 h, after which the catalyst was exposed to 100% $H_2$ for 12 h for the reduction. Catalytic testing of the competitive reaction feed, consisting of 2 wt % octyne in 10 wt % octene (with hexane as a diluent), and a full optimization study investigating the noncompetitive hydrogenation of octyne in hexane was carried out. For the latter, parameters such as temperature (40, 8, 100, 120, and 140 °C), pressure (10, 30, and 50 bar), LHSV (9, 18, 27, and 36 $h^{-1}$), octyne/$H_2$ ratio (1:1.5, 1:2, and 1:3.5), and Ag loading (2, 5, and 10 wt %) were varied to identify the best-performing catalyst and best potential conditions for application with the competitive feed. The product streams were quantified by a PerkinElmer Clarus 580 Auto System gas chromatograph integrated with a flame ionization detector (FID) and equipped with a PONA column (50 m × 0.2 mm × 0.5 $\mu$m). The column temperature program consisted of heating isothermally at 40 °C for 15 min, followed by a temperature ramp at 5 °C/min to 120 °C for 3 min, then at 5 °C/min to 200 °C for 2 min, and finally at 20 °C/min to 260 °C for 3


https://doi.org/10.1021/acsomega.1c05231
ACS Omega 2022, 7, 4026−4040

min. Results were obtained in at least duplicate with mass balances between 94 and 103% and carbon balances between 92 and 107%. Substrate conversion for the noncompetitive hydrogenation reaction was calculated by the difference in initial and final octyne molar amounts ($n_{octyne,in}$ and $n_{octyne,out}$, respectively) relative to the initial molar amount of octyne (eq 2):

$$\text{conversion} = \frac{n_{octyne,in} - n_{octyne,out}}{n_{octyne,in}} \times 100 \quad (2)$$

Product selectivities were calculated from the molar amounts of the individual products $k$ formed ($n_k$) relative to the total amount of all products formed in the product stream ($n_{products,total}$) (eq 3):

$$\text{selectivity}_{(noncompetitive\ feed)} = \frac{n_k}{n_{products,total}} \times 100 \quad (3)$$

For the competitive hydrogenation reaction, the octyne conversion was calculated in the same way as for the noncompetitive reaction. However, selectivities were based on the molar amount of octene (the substrate initially co-fed with octyne) gained as a product ($n_{1\text{-octene}}$) as well as the molar amounts of isomeric octene products ($n_{internal\ octenes}$) and the overhydrogenation product octane ($n_{octane}$) relative to the total amount of products formed (eq 4):

$$\text{total } C_8 \text{ selectivity}_{(competitive\ feed)} = \frac{n_{1\text{-octene}} + n_{internal\ octenes} + n_{octane}}{n_{products,total}} \times 100 \quad (4)$$

The gain of octene was based on the mass of octene detected by GC and inclusive of the initial octene fed ($m_{octene,out}$) and the mass of octene initially fed ($m_{octene,in}$) (eq 5):

$$\text{octene gain} = \frac{(m_{octene,out} - m_{octene,in})}{m_{octene,in}} \times 100 \quad (5)$$

## ■ ASSOCIATED CONTENT

### Supporting Information

The Supporting Information is available free of charge at https://pubs.acs.org/doi/10.1021/acsomega.1c05231.

Experimental setup as well as additional characterization techniques, i.e., $H_2$ chemisorption, powder XRD, and IR spectroscopy of all fresh catalysts, TGA−DSC of both fresh and used catalysts, Raman spectroscopy and TPO-MS of selected used catalysts, and SEM and TEM micrographs (PDF)

## ■ AUTHOR INFORMATION


### Corresponding Author

**Holger B. Friedrich** − *School of Chemistry and Physics, University of KwaZulu-Natal, Durban 4000, South Africa;* orcid.org/0000-0002-1329-0815; Phone: +27 31 2603107; Email: friedric@ukzn.ac.za

### Authors

**Revana Chanerika** − *School of Chemistry and Physics, University of KwaZulu-Natal, Durban 4000, South Africa*

**Mzamo L. Shozi** − *School of Chemistry and Physics, University of KwaZulu-Natal, Durban 4000, South Africa;* orcid.org/0000-0001-7666-2543

Complete contact information is available at: https://pubs.acs.org/10.1021/acsomega.1c05231


### Notes

The authors declare no competing financial interest.

## ■ ACKNOWLEDGMENTS

The authors are grateful to the University of KwaZulu-Natal and the NRF (grant 111660) for financial assistance. They gratefully acknowledge Dr. Alisa Govender and Dr. Matthew Coombes at Group Technology (SASOL South Africa, Pty Ltd.) for their assistance with microscopy characterization.

## ■ REFERENCES


(1) Molnár, Á.; Sárkány, A.; Varga, M. Hydrogenation of carbon−carbon multiple bonds: chemo-, regio- and stereo-selectivity. *J. Mol. Catal. A: Chem.* **2001**, *173*, 185−221.

(2) Andrade Sales, E.; Benhamida, B.; Caizergues, V.; Lagier, J.-P.; Fiévet, F.; Bozon- Verduraz, F. Alumina-supported Pd, Ag and Pd−Ag catalysts: Preparation through the polyol process, characterization and reactivity in hexa-1,5-diene hydrogenation. *Appl. Catal., A* **1998**, *172*, 273−283.

(3) Jin, Y.; Datye, A. K.; Rightor, E.; Gulotty, R.; Waterman, W.; Smith, M.; Holbrook, M.; Maj, J.; Blackson, J. The Influence of Catalyst Restructuring on the Selective Hydrogenation of Acetylene to Ethylene. *J. Catal.* **2001**, *203*, 292−306.

(4) Khan, N. A.; Shaikhutdinov, S.; Freund, H. J. Acetylene and Ethylene Hydrogenation on Alumina Supported Pd-Ag Model Catalysts. *Catal. Lett.* **2006**, *108*, 159−164.

(5) Kang, J. H.; Shin, E. W.; Kim, W. J.; Park, J. D.; Moon, S. H. Selective hydrogenation of acetylene on Pd/SiO2 catalysts promoted with Ti, Nb and Ce oxides. *Catal. Today* **2000**, *63*, 183−188.

(6) Burdick, D. L.; Leffler, D. L. *Petrochemicals in Nontechnical Language*, 2nd ed.; Pennwell Books: Tulsa, Oklahoma, United States, 1990; p 360.

(7) Nikolaev, S. A.; Smirnov, V. V. Synergistic and size effects in selective hydrogenation of alkynes on gold nanocomposites. *Catal. Today* **2009**, *147*, S336−S341.

(8) Teschner, D.; Vass, E.; Hävecker, M.; Zafeiratos, S.; Schnörch, P.; Sauer, H.; Knop-Gericke, A.; Schlögl, R.; Chamam, M.; Wootsch, A.; Canning, A. S.; Gamman, J. J.; Jackson, S. D.; McGregor, J.; Gladden, L. F. Alkyne hydrogenation over Pd catalysts: A new paradigm. *J. Catal.* **2006**, *242*, 26−37.

(9) Huang, D. C.; Chang, K. H.; Pong, W. F.; Tseng, P. K.; Hung, K. J.; Huang, W. F. Effect of Ag-promotion on Pd catalysts by XANES. *Catal. Lett* **1998**, *53*, 155−159.

(10) Hamilton, C. A.; Jackson, S. D.; Kelly, G. J.; Spence, R.; de Bruin, D. Competitive reactions in alkyne hydrogenation. *Appl. Catal., A* **2002**, *237*, 201−209.

(11) Kim, W. J.; Kang, J. H.; Ahn, I. Y.; Moon, S. H. Deactivation behavior of a TiO2- added Pd catalyst in acetylene hydrogenation. *J. Catal.* **2004**, *226*, 226−229.

(12) Panpranot, J.; Kontapakdee, K.; Praserthdam, P. Selective hydrogenation of acetylene in excess ethylene on micron-sized and nanocrystalline TiO2 supported Pd catalysts. *Appl. Catal., A* **2006**, *314*, 128−133.

(13) Kang, J. H.; Shin, E. W.; Kim, W. J.; Park, J. D.; Moon, S. H. Selective Hydrogenation of Acetylene on TiO2-Added Pd Catalysts. *J. Catal.* **2002**, *208*, 310−320.

(14) Borodziński, A.; Bond, G. C. Selective Hydrogenation of Ethyne in Ethene-Rich Streams on Palladium Catalysts. Part 1. Effect of Changes to the Catalyst During Reaction. *Cat. Rev.* **2006**, *48*, 91−144.

(15) Zaitseva, N. A.; Molchanov, V. V.; Chesnokov, V. V.; Buyanov, R. A.; Zaikovskii, V. I. Effect of the Nature of Coke-Forming Species on the Crystallographic Characteristics and Catalytic Properties of

Metal−Filamentous Carbon Catalysts in the Selective Hydrogenation of 1,3-Butadiene. *Kinet. Catal.* **2003**, *44*, 129−134.
(16) Wilhite, B. A.; McCready, M. J.; Varma, A. Kinetics of Phenylacetylene Hydrogenation over Pt/γ-Al2O3 Catalyst. *Ind. Eng. Chem. Res.* **2002**, *41*, 3345−3350.
(17) Sarkany, A. Semi-hydrogenation of 1,3-butadiene on adspecies modified Pd—Ni, Co and Cu catalysts. *Appl. Catal., A* **1997**, *149*, 207−223.
(18) Sárkány, A.; Révay, Z. Some features of acetylene and 1,3-butadiene hydrogenation on Ag/SiO2 and Ag/TiO2 catalysts. *Appl. Catal., A* **2003**, *243*, 347−355.
(19) Okumura, M.; Akita, T.; Haruta, M. Hydrogenation of 1,3-butadiene and of crotonaldehyde over highly dispersed Au catalysts. *Catal. Today* **2002**, *74*, 265−269.
(20) Choudhary, T. V.; Sivadinarayana, C.; Datye, A. K.; Kumar, D.; Goodman, D. W. Acetylene Hydrogenation on Au-Based Catalysts. *Catal. Lett* **2003**, *86*, 1−8.
(21) Pellegatta, J.-L.; Blandy, C.; Collière, V.; Choukroun, R.; Chaudret, B.; Cheng, P.; Philippot, K. Catalytic investigation of rhodium nanoparticles in hydrogenation of benzene and phenylacetylene. *J. Mol. Catal. A: Chem.* **2002**, *178*, 55−61.
(22) Dobrovolná, Z.; Kačer, P.; Červený, L. Competitive hydrogenation in alkene− alkyne−diene systems with palladium and platinum catalysts1This work is a part of the Selective Catalytic Hydrogenation and Transfer Hydrogenation project GA CR 104/96/1445.1. *J. Mol. Catal. A: Chem.* **1998**, *130*, 279−284.
(23) Thomas, J. M.; Thomas, W. J. *Introduction of the Principles of Heterogeneous Catalysis*; Academic Press: London, 1967.
(24) Fang, G.; Bi, X. Silver-catalysed reactions of alkynes: recent advances. *Chem. Soc. Rev.* **2015**, *44*, 8124−8173.
(25) Kannisto, H.; Arve, K.; Pingel, T.; Hellman, A.; Härelind, H.; Eränen, K.; Olsson, E.; Skoglundh, M.; Murzin, D. Y. On the performance of Ag/Al2O3 as a HC-SCR catalyst − influence of silver loading, morphology and nature of the reductant. *Catal. Sci. Technol.* **2013**, *3*, 644−653.
(26) Bethke, K. A.; Kung, H. H. Supported Ag Catalysts for the Lean Reduction of NO with C3H6. *J. Catal.* **1997**, *172*, 93−102.
(27) Furusawa, T.; Seshan, K.; Lercher, J.; Lefferts, L.; Aika, K.-i. Selective reduction of NO to N2 in the presence of oxygen over supported silver catalysts. *Appl. Catal., B* **2002**, *37*, 205−216.
(28) Wang, F.; Ma, J.; He, G.; Chen, M.; Zhang, C.; He, H. Nanosize Effect of Al2O3 in Ag/Al2O3 Catalyst for the Selective Catalytic Oxidation of Ammonia. *ACS Catal.* **2018**, *8*, 2670−2682.
(29) Edvardsson, J.; Rautanen, P.; Littorin, A.; Larsson, M. Deactivation and coke formation on palladium and platinum catalysts in vegetable oil hydrogenation. *J. Am. Oil Chem. Soc.* **2001**, *78*, 319−327.
(30) Jackson, S. D.; Casey, N. J. Hydrogenation of propyne over palladium catalysts. *J. Chem. Soc., Faraday Trans.* **1995**, *91*, 3269−3274.
(31) Garba, M. D.; Jackson, S. D. Catalytic upgrading of refinery cracked products by trans-hydrogenation: a review. *Appl. Petrochem. Res.* **2017**, *7*, 1−8.
(32) Delgado, J. A.; Benkirane, O.; Claver, C.; Curulla-Ferré, D.; Godard, C. Advances in the preparation of highly selective nanocatalysts for the semi-hydrogenation of alkynes using colloidal approaches. *Dalton Trans.* **2017**, *46*, 12381−12403.
(33) Cao, Y.; Sui, Z.; Zhu, Y.; Zhou, X.; Chen, D. Selective Hydrogenation of Acetylene over Pd-In/Al2O3 Catalyst: Promotional Effect of Indium and Composition- Dependent Performance. *ACS Catal* **2017**, *7*, 7835−7846.
(34) Nikolaev, S. A.; Zanaveskin, L.; Smirnov, V. V.; Averyanov, V. A.; Zanaveskin, K. Catalytic hydrogenation of alkyne and alkadiene impurities from alkenes. Practical and theoretical aspects. *Russ. Chem. Rev.* **2009**, *78*, 231−247.
(35) Ryu, J. Process for the Selective Hydrogenation of Alkynes. U.S. Patent US2004/0092783 A12004.
(36) McCue, A. J.; Guerrero-Ruiz, A.; Ramirez-Barria, C.; Rodríguez-Ramos, I.; Anderson, J. A. Selective hydrogenation of mixed alkyne/alkene streams at elevated pressure over a palladium sulfide catalyst. *J. Catal.* **2017**, *355*, 40−52.
(37) Parera, J. M. Deactivation and Regeneration of Pt-Re/Al2O3 Catalysts. In *Studies in Surface Science and Catalysis*; Elsevier, 1991; Vol. *68*, pp 103−109.
(38) Larsson, M.; Jansson, J.; Asplund, S. The Role of Coke in Acetylene Hydrogenation on Pd/α-Al2O3. *J. Catal.* **1998**, *178*, 49−57.
(39) Pachulski, A.; Schödel, R.; Claus, P. Kinetics and reactor modeling of a Pd- Ag/Al2O3 catalyst during selective hydrogenation of ethyne. *Appl. Catal., A* **2012**, *445−446*, 107−120.
(40) Nikolaev, S.; Zanaveskin, L.; Smirnov, V.; Averyanov, V.; Zanaveskin, K. Catalytic hydrogenation of alkyne and alkadiene impurities in alkenes. Practical and theoretical aspects. *Russ. Chem. Rev.* **2009**, *78*, 231−247.
(41) Ibhadon, A.; Kansal, S. The Reduction of Alkynes Over Pd-Based Catalyst Materials - A Pathway to Chemical Synthesis. *Chem. Eng. Technol.* **2017**, DOI: 10.4172/2157-7048.1000376.
(42) Simonovis, J.; Tillekaratne, A.; Zaera, F. The Role of Carbonaceous Deposits in Hydrogenation Catalysis Revisited. *J. Phys. Chem. C.* **2017**, *121*, 2285−2293.
(43) Bos, A. N. R.; Westerterp, K. R. Mechanism and kinetics of the selective hydrogenation of ethyne and ethene. *Chem. Eng. Process.* **1993**, *32*, 1−7.
(44) Velasco-Vélez, J. J.; Teschner, D.; Girgsdies, F.; Hävecker, M.; Streibel, V.; Willinger, M. G.; Cao, J.; Lamoth, M.; Frei, E.; Wang, R.; Centeno, A.; Zurutuza, A.; Hofmann, S.; Schlögl, R.; Knop-Gericke, A. The Role of Adsorbed and Subsurface Carbon Species for the Selective Alkyne Hydrogenation Over a Pd- Black Catalyst: An Operando Study of Bulk and Surface. *Top. Catal.* **2018**, *61*, 2052−2061.
(45) Ghosh, R.; Bandyopadhyay, A. R.; Jasra, R.; Gagjibhai, M. M. Mechanistic Study of the Oligomerization of Olefins. *Ind. Eng. Chem. Res.* **2014**, *53*, 7622−7628.
(46) Zhang, Q.; Li, J.; Liu, X.; Zhu, Q. Synergetic effect of Pd and Ag dispersed on Al2O3 in the selective hydrogenation of acetylene. *Appl. Catal., A* **2000**, *197*, 221−228.
(47) Kuhn, M.; Lucas, M.; Claus, P. Long-Time Stability vs Deactivation of Pd− Ag/Al2O3 Egg-Shell Catalysts in Selective Hydrogenation of Acetylene. *Ind. Eng. Chem. Res.* **2015**, *54*, 6683−6691.
(48) Takht Ravanchi, M.; Sahebdelfar, S. Pd-Ag/Al2O3 catalyst: Stages of deactivation in tail-end acetylene selective hydrogenation. *Appl. Catal., A* **2016**, *525*, 197−203.
(49) Vogelaar, B. M.; van Langeveld, A. D.; Eijsbouts, S.; Moulijn, J. A. Analysis of coke deposition profiles in commercial spent hydroprocessing catalysts using Raman spectroscopy. *Fuel* **2007**, *86*, 1122−1129.
(50) Matsushita, K.; Hauser, A.; Marafi, A.; Koide, R.; Stanislaus, A. Initial coke deposition on hydrotreating catalysts. Part 1. Changes in coke properties as a function of time on stream. *Fuel* **2004**, *83*, 1031−1038.
(51) Lynch, S. P. Metallographic and Fractographic Techniques for Characterising and Understanding Hydrogen-Assisted Cracking of Metals. In *Gaseous Hydrogen Embrittlement of Materials in Energy Technologies*; Gangloff, R. P.; Somerday, B. P., Eds.; Woodhead Publishing, 2012; Chapter 9, Vol. 2, pp 274−346.


https://doi.org/10.1021/acsomega.1c05231
*ACS Omega* 2022, 7, 4026−4040